Neutron-scattering study of spin fluctuations in superconducting $YBa_2Cu_3O_{6+x}$ ($x=0.40,0.45,0.50$)

Henry Chou, J. M. Tranquada, and G. Shirane
Physics Department, Brookhaven National Laboratory, Upton, New York 11973

T. E. Mason*
Physics Department, McMaster University, Hamilton, Ontario, Canada L8S 4M1

W. J. L. Buyers
AECL Research, Chalk River, Ontario, Canada K0J 1J0

S. Shamoto† and M. Sato
Department of Physics, Faculty of Science, Nagoya University, Furo-cho, Chikusa-ku, Nagoya 464-01, Japan
(Received 31 August 1990; revised manuscript received 12 December 1990)

We show by inelastic neutron scattering that dynamic spin correlations coexist with superconductivity in $YBa_2Cu_3O_{6+x}$ ($x=0.4,0.45,0.5$). For the $x=0.5$, $T_c=50$ K sample, the inelastic magnetic intensity at $\Delta E=6$ meV does not show any change near T_c and is approximately constant from 250 to 10 K, in contrast to earlier data on superconducting $La_{1.85}Sr_{0.15}CuO_4$ ($T_c=35$ K) which showed a decrease of the integrated intensity at a temperature well above T_c. The inelastic magnetic cross section observed here can be consistently modeled as two-dimensional spin waves overdamped by short correlation lengths. The correlation length in the $x=0.5$ sample is an order of magnitude smaller than in the $x=0.40$ and $x=0.45$ samples, indicating a drastic disruption of planar copper spin-spin correlation upon hole doping. The present results are compared with recent NMR studies of $T_c=60$ K material.

I. INTRODUCTION

It is well established that the insulating phase of $La_{2-x}Sr_xCuO_4$ ($x\sim 0$) and $YBa_2Cu_3O_{6+x}$ ($x<0.4$) are antiferromagnetically ordered.[1-6] Above T_N, the spin-spin correlation length in the CuO_2 layers was found to be well described by the two-dimensional (2D), spin-$\frac{1}{2}$ Heisenberg model.[7,8] Birgeneau *et al.*[9] showed that there are substantial spin correlations in superconducting samples of $La_{2-x}Sr_xCuO_4$ even below T_c. Subsequently, in a more detailed study of a $La_{1.85}Sr_{0.15}CuO_4$ single crystal, it was found that the integrated magnetic intensity at $\Delta E=6$ meV had a marked decrease at a temperature well above T_c, whereas at $\Delta E=12$ meV it remained constant with temperature. This was interpreted as the opening of a gap in the spin excitation spectrum at a low energy.[10] Rossat-Mignod *et al.* have come to a similar conclusion in their study of a superconducting sample of $YBa_2Cu_3O_{6.45}$.[11]

A previous attempt at looking for magnetic fluctuations in the superconducting phase of $YBa_2Cu_3O_{6+x}$ was limited to low energies and did not observe any inelastic magnetic intensity.[12] NMR studies of oxygen and copper relaxation rates, however, imply that the antiferromagnetic spin fluctuations persist in superconducting samples.[13-16] In two recent papers,[17,18] we described our observation of spin fluctuations in three superconducting single crystals of $YBa_2Cu_3O_{6+x}$ ($x=0.4$, 0.45, and 0.50). There we argued that the low-energy magnetic scattering could be accounted for by 2D spin waves overdamped by a short correlation length in the CuO_2 planes. In the present paper, we present more details of our measurements on the above-mentioned samples, particularly the temperature dependence of the low-energy magnetic scattering.

II. SAMPLE CHARACTERISTICS AND EXPERIMENTAL DETAILS

Details of the crystal growth have been given elsewhere.[19] The oxygen contents were controlled by annealing in argon or oxygen atomsphere at 470–700 °C. The single crystals are labeled Nos. 27, 30, and 29, with oxygenation levels $\delta=0.40$, 0.45, and 0.50, respectively. The oxygen contents were determined by high-resolution measurements of the lattice constants together with the knowledge of their transition temperatures, the details of which are described in an earlier publication.[17] In Table I we summarize the important properties of our samples. Figure 1 shows a phase diagram of $YBa_2Cu_3O_{6+x}$, with the relative positions of our samples indicated.

The crystals were approximately 1 cm^3 in volume and contain a large fraction of uniquely oriented crystal blocks with a mosaic spread of $\sim 2°$. The transition temperatures were determined by ac susceptibility measurements.[17] These crystals show a less sharp transition than a polycrystalline sample of $YBa_2Cu_3O_7$. For the $\delta=0.40$ and 0.45 samples, the (200) and (020) Bragg peaks (which

TABLE I. Sample characteristics.

Label	Oxygenation level x	T_c (K)	Volume (cm^3)	Lattice constants (Å)
No. 27	0.40	25	0.9	$a=3.878$
				$b=3.856$
				$c=11.796$
No. 30	0.45	45	1.0	$a=3.878$
				$b=3.855$
				$c=11.744$
No. 29	0.50	50	1.0	$a=3.884$
				$b=3.846$
				$c=11.737$

are simultaneously present due to twinning) are not completely separated. These effects suggest that the $\delta=0.40$ and 0.45 samples may be inhomogeneous. This possibility would be consistent with a recent muon-spin-resonance (μSR) study[20] of a series of powder samples indicating static local magnetic order at $T<0.1$ K for samples with $\delta<0.5$; the static component was absent only in samples with $T_c>50$ K. This raises the serious and legitimate question of whether the magnetic scattering we observe is due to nonsuperconducting regions of the sample, or whether magnetism is present in the same regions of the sample as the superconductivity. Characterization of the Meissner fraction of each of our crystals is difficult because of their size. However, field-cooled, dc magnetization measurements in an 8-Oe field on pieces from the interior and exterior of a chunk broken off from the $x=0.50$ crystal clearly demonstrate bulk superconductivity. Transition temperatures in the pieces were identical, consistent with a homogeneous oxygen concentration throughout the sample. Furthermore, magnetic Bragg peaks are completely absent in all three of our samples. As Rossat-Mignod *et al.* demonstrated, magnetic Bragg peaks should be easily detectable even if a small fraction of the sample has long-range magnetic order.[21,22]

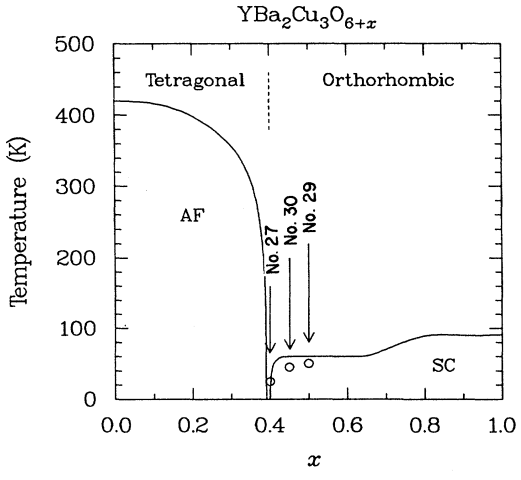

FIG. 1. Schematic phase diagram of $YBa_2Cu_3O_{6+x}$ showing the relative positions of the three samples studied here.

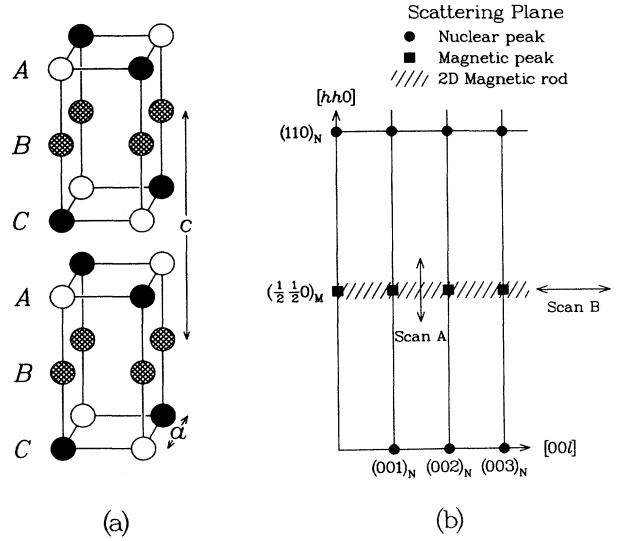

FIG. 2. (a) Antiferromagnetic structure of $YBa_2Cu_3O_{6+x}$. (b) Reciprocal lattice of $YBa_2Cu_3O_{6+x}$ in the $[hhl]$ zone.

The measurements to be discussed here were carried out at Brookhaven National Laboratory and at Chalk River Laboratories in Canada. For the $x=0.40$ ($T_c=25$ K) sample, the data presented here were collected at the High Flux Beam Reactor of Brookhaven National Laboratory, with pyrolytic graphite as monochromator as well as analyzer, and a collimator sequence of 40'-80'-80'-80', at fixed final energy $E_f=13.7$ meV. For the $x=0.45$ ($T_c=45$ K) and $x=0.50$ ($T_c=50$ K) samples, most of the data presented here were collected at the NRU reactor of Chalk River Laboratories, with a strained Si(111) monochromator and pyrolytic graphite analyzer, at fixed final energy $E_f=14.5$ meV, and collimator sequences as indicated on the various figures shown in the subsequent sections. The energy resolution of the spectrometer in the configurations used is approximately 1.5 meV.

In all cases, the crystals were oriented with the $[1\bar{1}0]$ direction perpendicular to the scattering plane. Figure (2b) depicts the reciprocal lattice in the (hhl) zone. Scans of types A and B were made at various energy transfers to study the spin correlations.

III. RESULTS

Since the compositions of our samples are very close to the insulator-metal boundary in the phase diagram, it is helpful to review the established magnetic behavior of insulating $YBa_2Cu_3O_{6+x}$ ($x<0.4$) before discussing our data.

Generally, 2D magnetic ordering is manifested by a rod of magnetic intensity in reciprocal space. The spin-wave intensity along the rod should be uniform (apart from instrumental resolution effects). In $YBa_2Cu_3O_{6+x}$, there are two CuO_2 layers per unit cell separated along the c axis by a distance of $\sim 0.3c$ [Fig. 2(a)], so that the Cu atoms do not form a Bravais lattice. The spin-wave modes are split into acoustic and optic branches. Tran-

quada *et al.*[6] as well as Rossat-Mignod *et al.*[11] have inferred that the optic modes are at energies greater than 30 meV. Therefore, at low energies, one observes only acoustic modes modulated by an inelastic structure factor.[19,6] This modulation provides a signature of spin correlation between the bilayers. In insulating samples of $YBa_2Cu_3O_{6+x}$ ($x<0.4$), it was found that this modulation persisted above the 3D ordering temperature T_N, i.e., the bilayers remain antiferromagnetically correlated in the absence of long-range 3D order.[6]

Figure (3a) shows scans in the $x=0.4$ sample along $(\frac{1}{2},\frac{1}{2},l)$ where the ridge of magnetic scattering would occur in a 2D correlated sample. For comparison, Fig. 3(b) shows a similar scan in magnetically ordered $YBa_2Cu_3O_{6.3}$. It is important to note that, although the $x=0.4$ sample shows no long-range magnetic order (absence of magnetic Bragg peaks), the modulation due to the bilayer coupling is clearly evident. Similar modulation has been shown for the $x=0.45$ sample in a previous publication.[17] Furthermore, the additional modulations at $l=\pm 1.5$, which had been shown to be due to 3D dispersion effects of the in-plane acoustic spin-wave branch,[6] are also clearly observable. 3D dispersion suggests quite significant correlation lengths.

Constant-E scans in the $x=0.4$ sample across the 2D rod of $(\frac{1}{2},\frac{1}{2},l)$ at $\Delta E=6$ meV for several temperatures [scans of Type A in Fig. 2(b)] are shown in Fig 4(a). The intensity and the inverse linewidth decrease slightly with increasing temperature. Figure (4b) shows the energy dependence of the magnetic intensity at $\mathbf{Q}=(\frac{1}{2},\frac{1}{2},-1.8)$. This energy dependence is similar to that of insulating $YBa_2Cu_3O_{6.3}$, with the important difference that it tends to peak at a somewhat higher energy than the insulator. This indicates that the magnetic intensity observed here is not due to magnetic impurities in the sample, in which

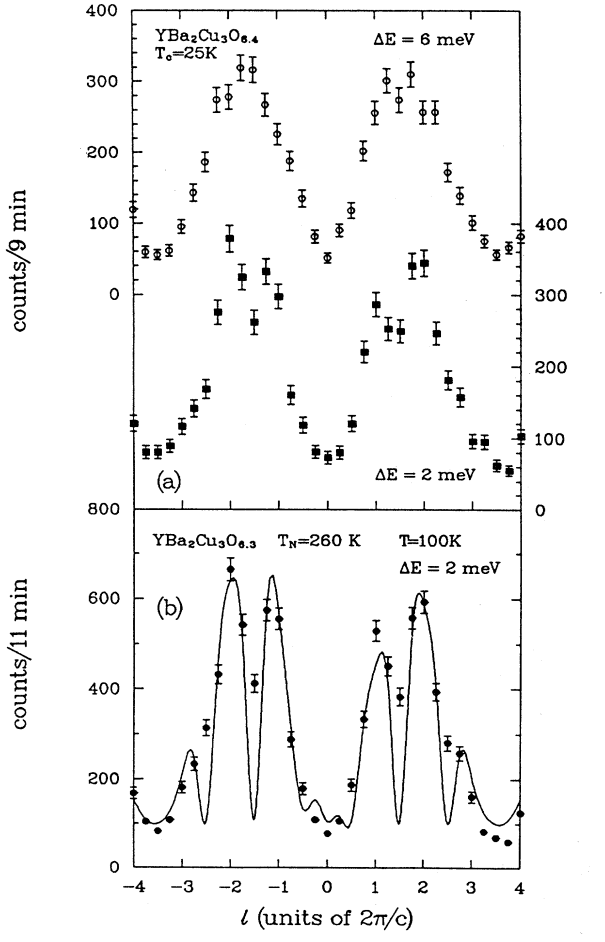

FIG. 3. (a) Scans along $(\frac{1}{2},\frac{1}{2},l)$ at energy transfers $\Delta E=2$ and 6 meV for the $T_c=25$ K sample. The features at $l=\pm 1.5$ are due to 3D dispersion effect. (b) For comparison, a similar scan at $\Delta E=2$ meV for an insulating sample $YBa_2Cu_3O_{6.3}$. The solid line is calculated from a cross section including the bilayer coupling $\sin(\pi z' l)$, where $z'=1-2z$ and z is the fraction of a unit-cell length by which the bilayers are separated (from Ref. 6).

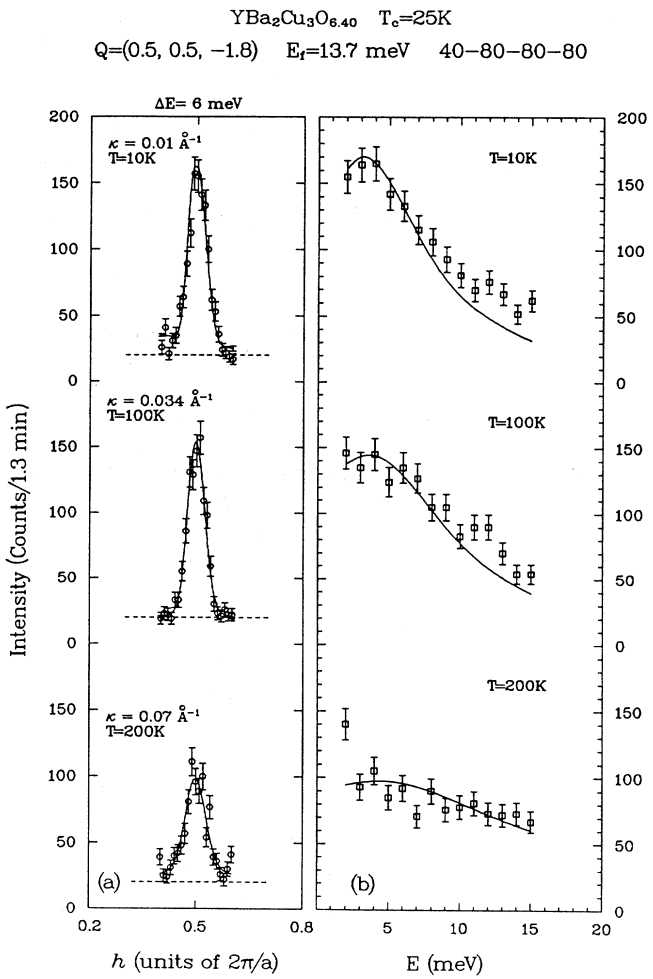

FIG. 4. (a) Constant-E scans for the $T_c=25$ K sample at $\Delta E=6$ meV. The dashed lines represent the estimated background. The solid lines are fits using Eq. (4) with the fit parameters listed in Table II. (b) Energy dependence of magnetic intensity at $\mathbf{Q}=(\frac{1}{2},\frac{1}{2},-1.8)$. The behavior is similar to the $T_c=45$ K sample.

case the energy dependence should peak at $\Delta E = 0$. Our understanding of the peak in the energy dependence at a small but nonzero energy will be discussed in the next section. Figure 5 shows similar constant-E scans as in Fig. 4(a) but for the $x = 0.45$ sample.

The $x = 0.5$ sample shows behavior considerably different from the $x = 0.4$ and 0.45 samples. The constant-E scans are significantly broader than those of the other two samples. Figure 6 shows the constant-E scans from the $x = 0.5$ sample across the $(\frac{1}{2}, \frac{1}{2}, l)$ rod at several energy transfers and temperatures. As will be discussed in the next section, the magnetic intensities can be consistently modeled as 2D spin waves overdamped by short correlation lengths. The in-plane spin-spin correlation length of the $x = 0.5$ sample is shorter than those of

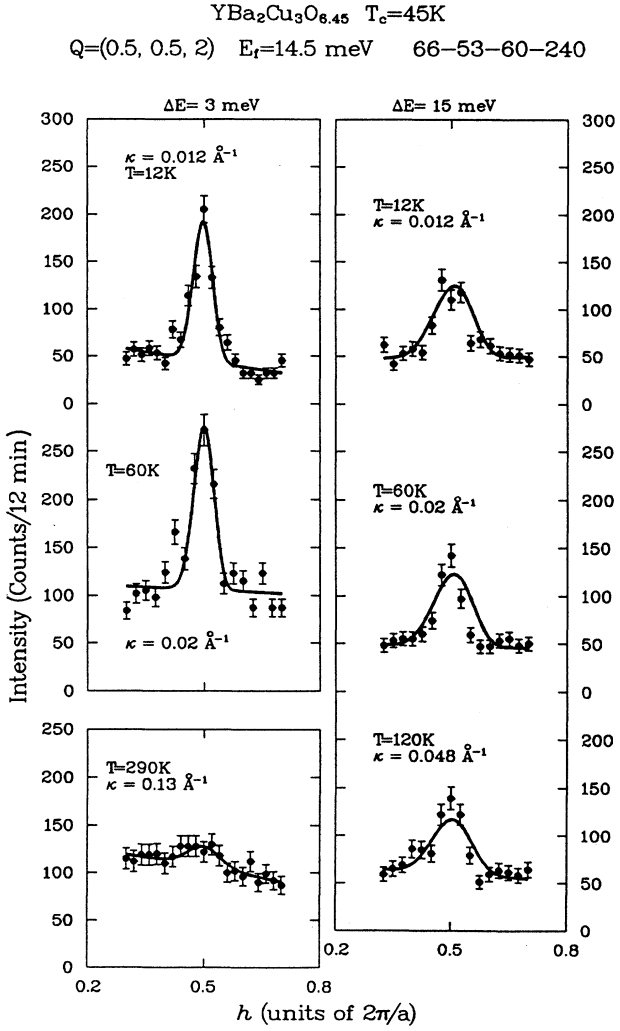

FIG. 5. Constant-E scans for the $T_c = 45$ K sample at $\Delta E = 3$ and 15 meV, and several temperatures. The fit parameters are listed in Table II. The higher background at $\Delta E = 3$ meV and $T \geq 60$ K is probably due to nitrogen gas inadvertently present in the sample container. At $\Delta E = 3$ meV, there is no data available at $T = 120$ K. The spectrum at the lower left was taken at $T = 290$ K.

the $x = 0.40$ and 0.45 samples by as much as an order of magnitude. Interestingly, there is evidence of interplanar correlation even below T_c, as indicated by constant-E scans along $(\frac{1}{2}, \frac{1}{2}, l)$ shown in Fig. 7(a). It is extremely surprising that even though the in-plane correlation length is only a few cell lengths, spins in neighboring planes nevertheless remain dynamically correlated. For comparison, Fig. 7(b) shows a similar scan for insulating $YBa_2Cu_3O_{6.3}$ above its Néel temperature.

Figure 8 shows the temperature dependence of the peak magnetic intensity at $Q = (\frac{1}{2}, \frac{1}{2}, 2)$. There is no change of the magnetic intensity at T_c. In fact, it is practically constant throughout the entire temperature range studied. In constrast, in a $La_{1.85}Sr_{0.15}CuO_4$ sample, Shirane *et al.*[10] observed a sharp decrease of integrated magnetic intensity well above the T_c of that sample. A similar decrease of intensity in $YBa_2Cu_3O_{6.45}$ ($T_c = 34.8$ K) was reported by Rossat-Mignod *et al.*[11] The temperature-independent magnetic intensity in our $x = 0.5$ sample can be explained by a correlation length decreasing with increasing temperature, as will be discussed in the next section.

The most striking feature of the $x = 0.5$ sample is the energy dependence of its magnetic cross section. In Fig. 9, this is contrasted with that of the $x = 0.45$ sample. Instead of peaking at a low energy, it is substantially suppressed at low energies, rising to a level comparable to that of the $x = 0.45$ sample at higher energies. Unfortunately, our scattering geometry at $\mathbf{Q} = (\frac{1}{2}, \frac{1}{2}, 1.8)$ limited our energy range because, at high-energy transfers, we would get too much noise from small-angle scattering. A larger Q would have allowed us to go further in energy but the intensity there would be weaker. We thus were not able to go to high enough energy to tell if the inelastic magnetic cross section actually peaks and then decreases.

IV. DATA ANALYSIS AND DISCUSSION

The differential scattering cross section for neutrons is proportional to the scattering function $S(\mathbf{q},\omega)$, which in turn is proportional to the imaginary part of the generalized susceptibility $\chi''(\mathbf{q},\omega)$ multiplied by a thermal population factor,

$$S(\mathbf{q},\omega) \sim [n(\omega)+1]\chi''(\mathbf{q},\omega) , \quad (1)$$

where $n(\omega) = [\exp(\hbar\omega/k_B T) - 1]^{-1}$ is the Bose factor. The susceptibility contains the details of the interactions in the system being probed. The thermal factor is a monotonically increasing function of temperature. If the scattered intensity does not follow this behavior in temperature, then the susceptibility itself must be temperature dependent. As pointed out with Fig. 8(b), the peak intensity at $Q = (\frac{1}{2}, \frac{1}{2}, 2)$, after background correction, is almost constant in temperature. The thermal factor in Eq. (1) is an increasing function of temperature, as indicated by the dashed line in Fig. 8(b). The observed temperature-independent magnetic scattering in the $x = 0.5$ sample implies that its spin susceptibility must decrease with increasing temperature.

A simple way of modeling the temperature-dependent susceptibility is to consider correlated regions of Cu spins in the CuO_2 plane with a temperature-dependent correlation length. The correlated regions are capable of supporting short-wavelength (high-energy) 2D antiferromagnetic spin waves, while long-wavelength spin waves are overdamped by the limited correlation length. In other words, the inelastic magnetic cross section is suppressed at low energies, as indeed is the case for our $T_c = 50$ K sample (Fig. 9). This would also explain the failure of an earlier attempt to measure magnetic fluctuations at low energies.[12]

According to the above picture, we can write the inelastic magnetic cross section as

$$S(\mathbf{q},\omega) \sim \frac{1}{1-e^{-\hbar\omega/kT}} \frac{\hbar\omega}{\kappa^2+q^2} \left[\frac{\Gamma}{\Gamma^2+(\hbar\omega-\hbar\omega_q)^2} + \frac{\Gamma}{\Gamma^2+(\hbar\omega+\hbar\omega_q)^2} \right], \tag{2}$$

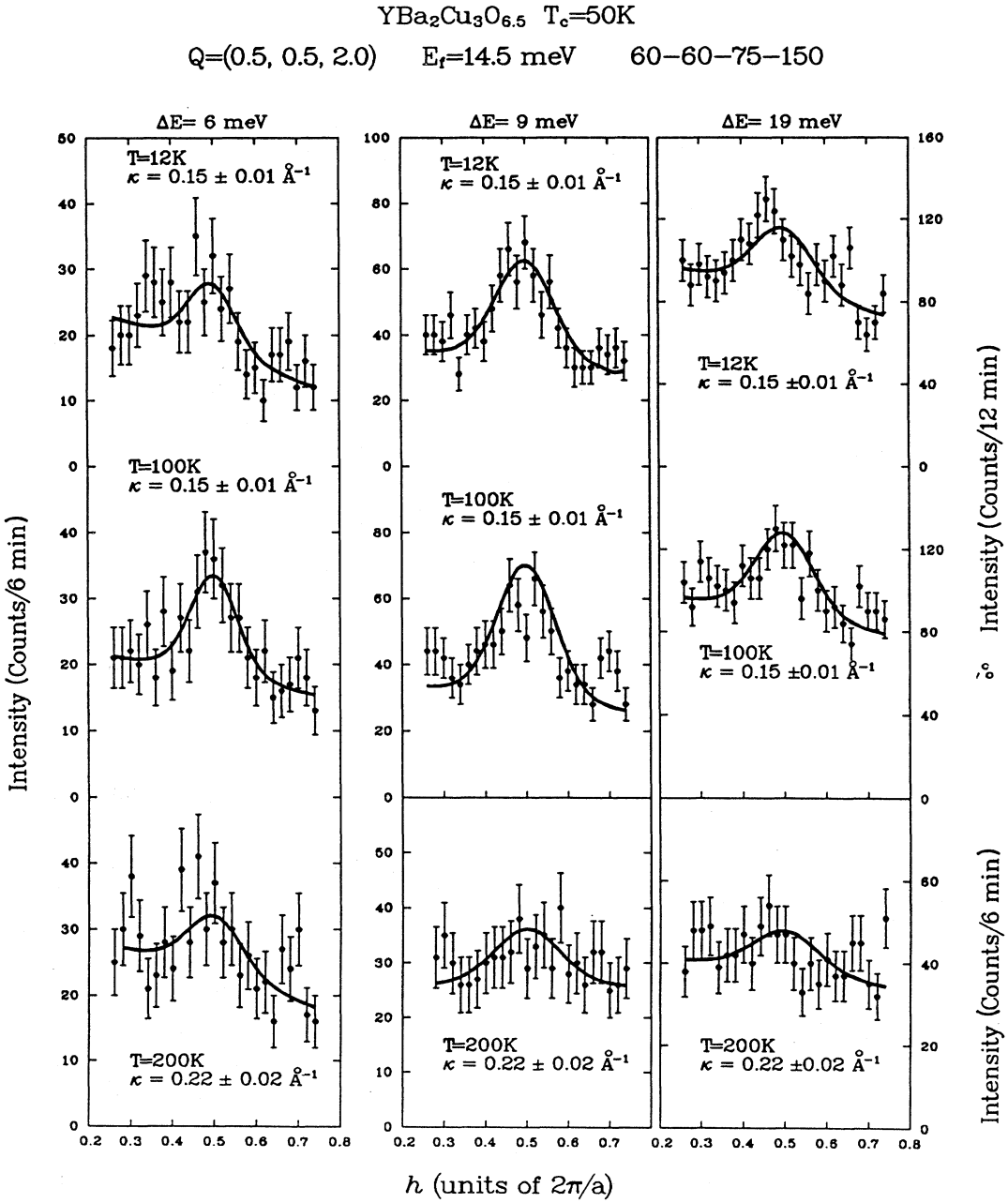

FIG. 6. Constant-E scans for the $x = 0.5$ ($T_c = 50$ K) sample at several energies and temperatures. The fit parameters are listed in Table II.

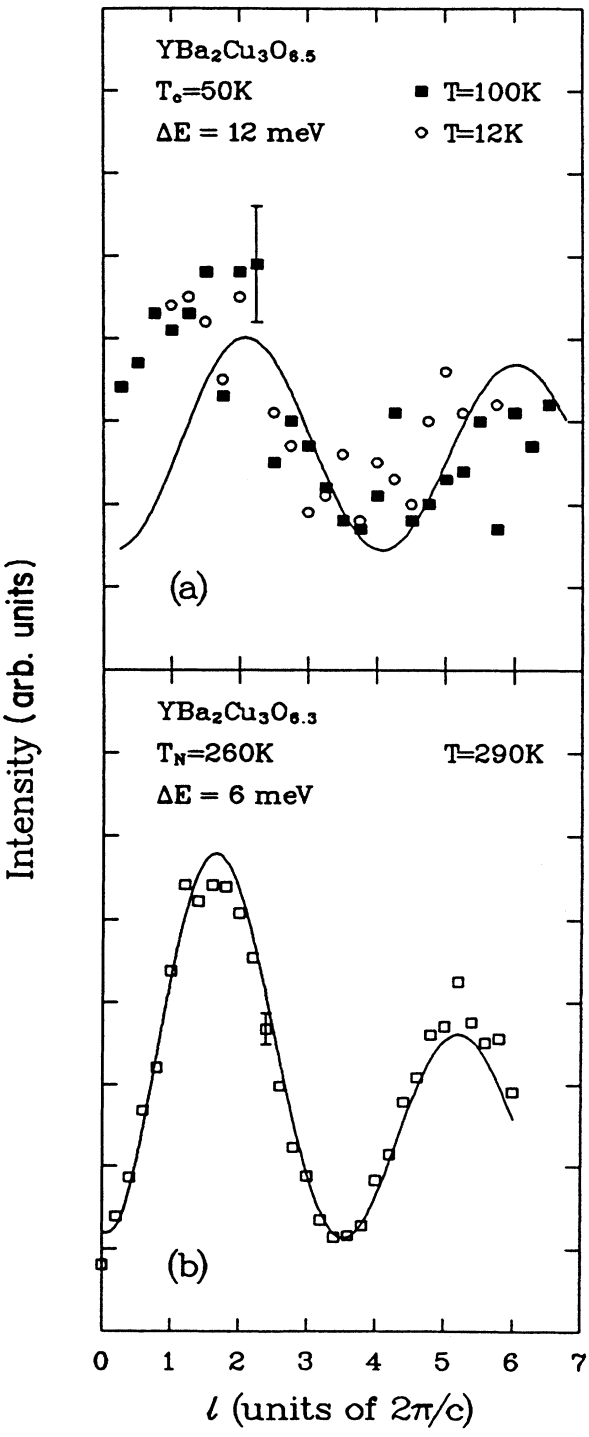

FIG. 7. (a) Scan along $(\frac{1}{2},\frac{1}{2},l)$ at energy transfer $\Delta E=12$ meV for the $T_c=50$ K sample. Both above and below T_c the modulation due to bilayer coupling is evident. The solid line is calculated from a cross section including the bilayer coupling $\sin(\pi z' l)$, where $z'=1-2z$ and $z=0.26$ is the fraction of a unit-cell length by which the bilayers are separated. (b) A similar scan at $\Delta E=6$ meV for an insulating sample above its Néel temperature (from Ref. 6). The solid line is calculated with $z=0.23$.

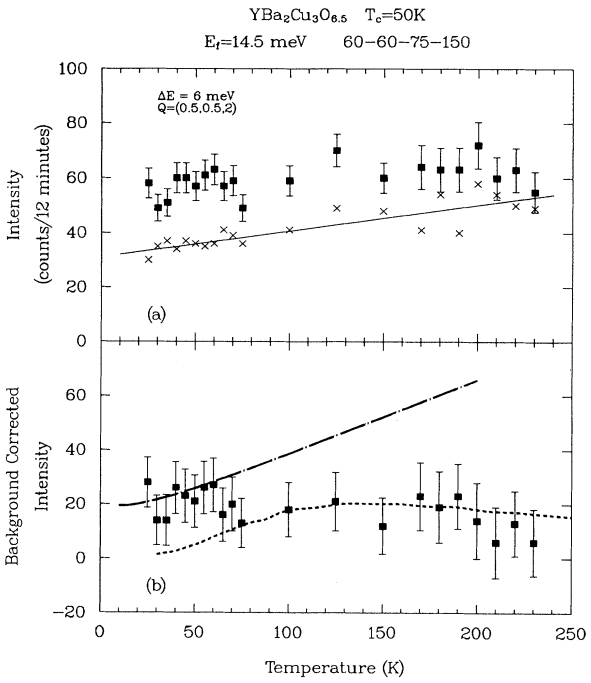

FIG. 8. (a) Temperature dependence of the magnetic intensity at $\mathbf{Q}=(\frac{1}{2},\frac{1}{2},2)$ and $\Delta E=6$ meV. The crosses are the background levels taken as the average of the intensities at $\mathbf{Q}=(0.2,0.2,2)$ and $\mathbf{Q}=(0.8,0.8,2)$. The solid line is a guide to the eye through the background points. (b) Background-corrected magnetic intensity from (a). The dot-dashed line is the thermal factor $B[n(\omega)+1]$ in Eq. (1), where B is a constant adjusted to make the line coincide with the data at low temperatures. The dashed line indicates the corresponding temperature dependence extracted from Cu nuclear spin relaxation rate measurements for a $T_c=60$ K sample, as discussed in the text.

where $q=|\mathbf{q}|=|\mathbf{Q}-\mathbf{Q}_{\rm rod}|$, $\mathbf{Q}$ is the scattering vector, $\mathbf{Q}_{\rm rod}=(\frac{1}{2},\frac{1}{2},l)$, $\hbar\omega_q=\hbar cq$ is the energy of the antiferromagnetic spin wave, and c is the spin-wave velocity. The part outside of the large parentheses can be thought of as the "paramagnetic" part due to limited correlation length. In this context, the parameter c, which we call "spin-wave velocity," should not be taken too literally. In Eq. (2), if one sets $\Gamma=\hbar c\kappa$, it becomes quite similar to the equation used by Tyc, Halperin, and Chakravarty to parametrize their numerical results for the 2D quantum Heisenberg antiferromagnet.[23] The constraint $\Gamma=\hbar c\kappa$ means that spin waves with wavelength longer than the correlation length $\xi=1/\kappa$ are suppressed. We note for future reference that at low temperatures and $\mathbf{q}=\mathbf{0}$, the above form becomes

$$S(\mathbf{q}=\mathbf{0},\omega)|_{T=0}\sim\frac{2\Gamma}{\kappa^2}\frac{\hbar\omega}{(\hbar\omega)^2+\Gamma^2} \tag{3}$$

which peaks at the energy $\hbar\omega=\Gamma$. This is important for fitting the energy dependence, as we will discuss later.

To fit our data, we use a cross section of the form given in Eq. (2) convolved with the instrumental resolution function. The constant-E scans shown in Fig. 6 are quite broad. In order to get reasonable fits, we would have to

use an unreasonably short correlation length $\xi=1/\kappa$. It is possible, however, that the large width is due to unresolved incommensurate spin structure. There is experimental evidence for 2D incommensurability in $La_{2-x}Sr_xCuO_4$,[9,10] as well as theoretical predictions[24,25] of spin canting which could lead to incommensurate inelastic scattering. We have taken such a possibility into account by allowing the spin waves to disperse out from an incommensurate position $\mathbf{q}=\mathbf{q}_{\rm inc}$ rather than $\mathbf{q}=\mathbf{0}$. In its full form, the inelastic cross section we used is

$$S(\mathbf{q},\omega)=\frac{A}{1-e^{-\hbar\omega/kT}}\frac{\hbar\omega}{\kappa^2+(q\pm q_{\rm inc})^2}\left[\frac{\Gamma}{\Gamma^2+[\hbar\omega-\hbar c(q\pm q_{\rm inc})]^2}+\frac{\Gamma}{\Gamma^2+[\hbar\omega+\hbar c(q\pm q_{\rm inc})]^2}\right]+B_1q_h+B_0\ , \tag{4}$$

where $q=(q_h^2+q_z^2)^{1/2}$, q_h is the component of $\mathbf{q}$ in the scattering plane and q_z is the out-of-plane component. The parameters are A = amplitude ($\propto$ total number of moments contributing to magnetic scattering), κ = inverse correlation length, $q_{\rm inc}$ = incommensurate wave vector, c = spin-wave velocity, and the background terms are B_0 and B_1.

Because of the large number of parameters, it is important to keep in mind the constraints and consistency checks that have to be satisfied. Firstly, the most important consistency check is that the same set of parameters have to fit not only the q dependence [Figs. 4(a), 5, and 6] but also the energy dependences [Figs. 4(b) and 9]. Secondly, as discussed in the preceding two paragraphs, we kept the constraint $\Gamma=\hbar c\kappa$. As we pointed out with Eq. (3), Γ is where the cross section should peak in energy.

In carrying out our data analysis, we followed a general guideline. For each constant-E scan, the background terms B_0 and B_1 are first determined with a preliminary fit. They are not modified subsequently. Then, since we do not have sufficiently detailed data to determine the spin-wave velocity c, we choose by trial and error reasonable values of c and $q_{\rm inc}$ which combine to give approximately the observed q width. Finally, κ and A are varied by a least-squares procedure to give a good fit to the constant-E scans. κ is the only temperature-dependent parameter; A has no temperature dependence (by assumption). The parameters, once determined, are then used to calculate the energy dependences. The above procedure is iterated until a set of parameters is arrived at which give a consistent overall fit to all the data at the various temperatures studied. We emphasize that this procedure does not necessarily arrive at the optimal parameters, nor even a unique set of parameters, but gave a good overall consistency and physical meaningfulness of the parameters. The fitted curves are shown in Figs. 4, 5, 6, and 9 as solid lines and values of the fit parameters are summarized in Table II.

We would like to draw attention to two features in Table II. Firstly, for each sample, data at different energies and temperatures were fitted with the same parameters except the correlation length $\xi=1/\kappa$, which decreases with increasing temperatures. For the $x=0.50$ sample, this temperature dependence cancels that from the Bose factor, resulting in a temperature-independent $S(\mathbf{q},\omega)$. Secondly, the correlation lengths in the $x=0.40$ and 0.45 samples are an order of magnitude larger than

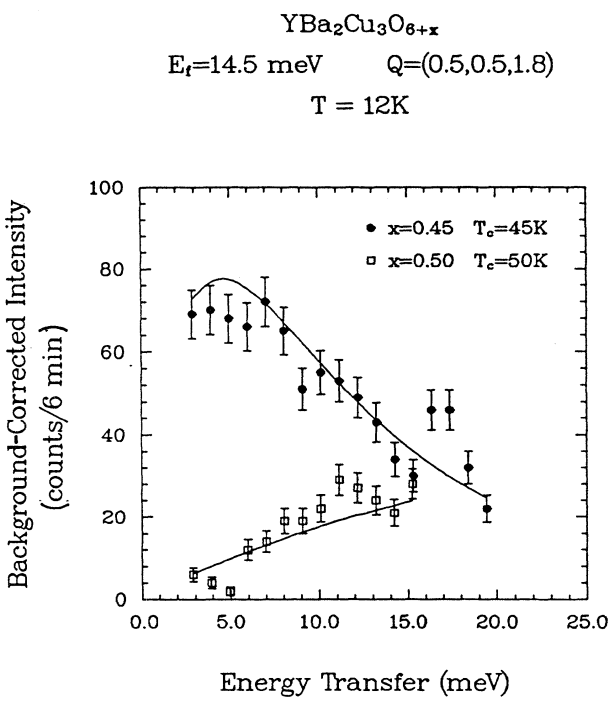

FIG. 9. Energy dependence of magnetic intensity at $\mathbf{Q}=(\frac{1}{2},\frac{1}{2},1.8)$ for the $T_c=45$ and 50 K samples. A constant background has been subtracted from each set of data. The intensity for the $T_c=50$ K sample is substantially suppressed at low energies. Note that the solid lines are calculated from parameter values deduced from fits to the constant-E scans (Figs. 5 and 6) with no further adjustments.

TABLE II. Fit parameters. The standard errors on the correlation lengths ξ are approximately $\pm 10\%$.

Sample	hc (meV Å)	$q_{\rm inc}$ (Å^{-1})	T (K)	$\xi=1/\kappa$ (Å)
$x=0.40$	100	0.01	10	100
$T_c=25$ K			100	30
			200	15
$x=0.45$	150	0.01	12	80
$T_c=45$ K			60	50
			120	20
$x=0.50$	200	0.05	12	7
$T_c=50$ K			100	7
			200	5

that of the $x=0.50$ sample. Since these samples fall in the region of phase diagram where the hole density is increasing rapidly,[26] this suggests a drastic disruption of spin-spin correlation length upon hole doping.

V. COMPARISON WITH NMR RESULTS

In NMR spectroscopy, one measures the spin-lattice relaxation rate, which is the low-frequency limit of the dynamical susceptibility averaged over the Brillouin zone,

$$\frac{1}{T_1}=k_B T\frac{\gamma}{2\mu_B^2}\lim_{\omega\to 0}\sum_q |A(q)|^2\frac{\chi''(q,\omega)}{\omega} , \tag{5}$$

where $A(q)$ is the hyperfine coupling between the electronic spin and the nuclear spin of gyromagnetic ratio γ. For conduction electrons in an ordinary metal, the susceptibility is temperature independent, hence the spin-lattice relaxation rate $1/T_1$ is proportional to temperature.

There have been a number of NMR studies of spin dynamics in $YBa_2Cu_3O_{6+x}$, initially on 90-K superconductors,[14–16,27–29] but more recently also on 60-K material.[13,27,28,30] It is the latter work with which we propose to compare the neutron-scattering results on our $T_c=50$ K crystal. Distinctly different spin relaxation rates are observed at the Cu and O sites. The general consensus is that the difference is due to the form factors for the two sites: The Cu form factor gives strong weight to the region of reciprocal space near the antiferromagnetic point where spin correlations cause a peak in $\chi''(\mathbf{q},\omega)$, whereas the O form factor is quite small in this region. We have observed the peak in the susceptibility directly with neutrons, as shown in Fig. 6. We would like to compare the temperature dependence of the Cu relaxation rate with the neutron-scattering measurement of $\chi''(\mathbf{q}=0,\omega)$, at $\hbar\omega=6$ meV. To make a proper comparison, one must take into account the $\mathbf{q}$ averaging in the NMR measurement, and this correction can only be done with a model for the susceptibility.

Monien, Pines, and Takigawa[31] have applied the model proposed by Millis, Monien, and Pines[32] to analyze NMR measurements on an $x=0.63$ sample by Takigawa *et al.*[30] In our notation their model susceptibility can be written

$$\chi''(\mathbf{q},\omega)=\chi_Q\frac{\omega\Gamma}{\omega^2+\Gamma^2(1+\xi^2q^2)^2} , \tag{6}$$

where $\Gamma\sim\xi^{-2}$ and both χ_Q and ξ are assumed to be temperature dependent. (Our Γ is different from the Γ of Monien, Pines, and Takigawa;[31] our Γ is equal to their ω_{SF}.) The temperature dependence of the Cu relaxation rate is given by

$$(^{63}T_1T)^{-1}\sim\chi_Q(T) ,$$

while for $\omega\ll\Gamma$ and $\mathbf{q}=\mathbf{0}$ one has

$$\chi''(\mathbf{0},\omega)\sim\chi_Q(T)\xi^2(T) .$$

Thus, for $\omega\sim 0$, as in the NMR measurements, one might expect

$$S(\mathbf{0},\omega)\sim\frac{T}{\omega}\chi''(\mathbf{0},\omega)\sim\xi^2(T)/^{63}T_1 ,$$

at least in the normal state.

Monien, Pines, and Takigawa[31] have extracted $\xi(T)$ for the normal state from their model-dependent analysis of the $T_c=60$ K NMR results. They find that $\xi(T)$ varies roughly linearly, decreasing by a factor of 2 in going from 60 to 300 K. To extrapolate below T_c, we will make the reasonable assumption that ξ remains constant at its 60-K value. We have taken the $(^{63}T_1)^{-1}$ data of Takigawa *et al.*,[30] multiplied it by $\xi^2(T)$, and plotted the results as a dashed line in Fig. 8(b). The comparison is limited by the statistics of the neutron-scattering data; nevertheless, the temperature dependence of the two sets of data is quite consistent throughout most of the normal state. It is only in the superconducting regime that a significant discrepancy appears. The data are not in direct conflict, since the NMR results correspond to $\omega=0$, while the neutron-scattering measurements correspond to $\hbar\omega=6$ meV. One might be tempted to explain the difference in terms of a gap at an intermediate energy scale. Indeed, Rossat-Mignod *et al.*[33] have reported a gap of ~ 4 meV in a crystal with $T_c=47$ K. However, keeping in mind that our measurements are at 6 meV $\ll 2\Delta_{\min}=3.5kT_c=15$ meV, a gap at such a small energy would be difficult to rationalize.

So far we have only compared temperature dependences. It is also of interest to compare the $(\mathbf{q},\omega)$ dependence of the Millis, Monien, and Pines model[32] with our results. Note that the frequency dependence is not tested or constrained by the NMR analysis, since those measurements all correspond to $\omega=0$. Since we observe no strong temperature dependence in the neutron-scattering data, we will compare our 12-K data for the $x=0.5$ crystal with the parameters extracted from the NMR data at 60 K for the $x=0.63$ sample by Monien, Pines, and Takigawa.[31] They find $\hbar\Gamma=\hbar\omega_{SF}=2.7$ meV, whereas we require $\hbar\Gamma=30$ meV to describe the data in Fig. 9. Thus, compared to their model, neutron-scattering indicates that the spin fluctuations are more strongly damped by an order of magnitude. As for the q dependence, they find a low-temperature value of $\xi=15$ Å. Fitting our constant-E scans with their model $\chi''(q,\omega)$, we find that the data are better described with $\xi\sim 7.5$ Å, but that we cannot rule out a value as large as 15 Å.

VI. CONCLUSION

It is evident from both neutron-scattering and NMR data that dynamic spin correlations persist in superconducting samples of $YBa_2Cu_3O_{6+x}$. It is not clear, however, whether a gap develops in the spin excitation spectrum. We did not observe any change in the inelastic magnetic intensity at $\Delta E=6$ meV near T_c, while the NMR spin-lattice relaxation rate $1/T_1$ shows a precipi-

tous drop near or below T_c. Recently it has been suggested[34,35] that in the superconducting state the dynamic structure factor $S(\mathbf{q},\omega)$ should vanish for $\hbar\omega < 2\Delta$. The data for our $x = 0.5$ sample at 12 K, for which $2\Delta > 15$ meV, are inconsistent with such models.

We have shown that the temperature and energy dependences of the magnetic scattering data can be explained without invoking a gap. A picture of magnetically correlated regions in the CuO_2 planes with a limited and temperature-dependent correlation length can reasonably account for all the data available so far. The temperature dependence of the neutron-scattering data at 6 meV is consistent with Cu nuclear relaxation rate measurements in the normal state; however, differences occur at low temperature. To clarify the situation, more neutron-scattering measurements are needed on samples with higher transition temperatures.

ACKNOWLEDGMENTS

We acknowledge the assistance of M. Nielsen and J. Als-Nielsen in characterizing the samples, and helpful discussions with V. J. Emery, S. M. Shapiro, S. K. Sinha, and J. Rossat-Mignod. This work was supported in part by the U.S.-Japan Collaborative Program on Neutron scattering. Work at Brookhaven was supported by the Division of Materials Science, U.S. Department of Energy, under Contract No. DE-AC02-76CH00016. T.E.M. acknowledges support by the Natural Sciences and Engineering Research Council of Canada.

*Present address: AT&T Bell Laboratories, 600 Mountain Ave., Murray Hill, NJ.

†Permanent address: Institute for Molecular Science, Okazaki 444, Japan.

[1]D. Vaknin, S. K. Sinha, D. E. Moncton, D. C. Johnston, J. M. Newsam, C. R. Safinya, and H. E. King, Jr., Phys. Rev. Lett. **58**, 2802 (1987).

[2]Y. Endoh, K. Yamada, R. J. Birgeneau, D. R. Gabbe, H. P. Jenssen, M. A. Kastner, C. J. Peters, P. J. Picone, T. R. Thurston, J. M. Tranquada, G. Shirane, Y. Hidaka, M. Oda, Y. Enomoto, M. Suzuki, and T. Murakami, Phys. Rev. B **37**, 7443 (1988).

[3]R J. Birgeneau and G. Shirane, in *Physical Properties of High Temperature Superconductors,* edited by D. M. Ginsberg (World Scientific, Singapore, 1989).

[4]J. M. Tranquada, D. E. Cox, W. Kunnmann, H. Moudden, G. Shirane, M. Suenaga, P. Zolliker, D. Vaknin, S. K. Sinha, M. S. Alvarez, A. J. Jacobson, and D. C. Johnston, Phys. Rev. Lett. **60**, 154 (1988).

[5]J. M. Tranquada, A. H. Moudden, A. I. Goldman, P. Zolliker, D. E. Cox, G. Shirane, S. K. Sinha, D. Vaknin, D. C. Johnston, M. S. Alvarez, A. J. Jacobson, J. T. Lewandowski, and J. M. Newsam, Phys. Rev. B **38**, 2477 (1988).

[6]J. M. Tranquada, G. Shirane, B. Keimer, S. Shamoto, and M. Sato, Phys. Rev. B **40**, 4503 (1989).

[7]S. Chakravarty, B. I. Halperin, and D. R. Nelson, Phys. Rev. Lett. **60**, 1057 (1988).

[8]S. Chakravarty, B. I. Halperin, and D. R. Nelson, Phys. Rev. B **39**, 2344 (1989).

[9]R. J. Birgeneau, Y. Endoh, K. Kakurai, Y. Hidaka, T. Murakami, M. A. Kastner, T. R. Thurston, G. Shirane, and K. Yamada, Phys. Rev. B **39**, 2868 (1989).

[10]G. Shirane, R. J. Birgeneau, Y. Endoh, P. Gehring, M. A. Kastner, K. Kitazawa, H. Kojima, I. Tanaka, T. R. Thurston, and K. Yamada, Phys. Rev. Lett. **63**, 330 (1989).

[11]J. Rossat-Mignod, L. P. Regnault, M. J. Jurgens, C. Vettier, P. Burlet, J. Y. Henry, and G. Lapertot, Physics B **163**, 4 (1990).

[12]T. Bruckel, H. Capellmann, W. Just, O. Scharpf, S. Kemmler-Sack, R. Kiemel, and W. Schaeffer, Europhys. Lett. **4**, 1189 (1987).

[13]W. W. Warren, Jr., R. E. Walstedt, G. F. Brennert, R. J. Cava, R. Tycko, R. F. Bell, and G. Gabbagh, Phys. Rev. Lett. **62**, 1193 (1989).

[14]C. H. Pennington, D. J. Durand, C. P. Slichter, J. P. Rice, E. D. Bukowski, and D. M. Ginsberg, Phys. Rev. B **39**, 274 (1989).

[15]M. Horvatic, P. Segransan, C. Berthier, Y. Berthier, P. Butaud, J. Y. Henry, M. Couach, and J. P. Chaminade, Phys. Rev. B **39**, 7332 (1989).

[16]P. C. Hammel, M. Takigawa, R. H. Heffner, Z. Fisk, and K. C. Ott, Phys. Rev. Lett. **63**, 1992 (1989).

[17]G. Shirane, J. Als-Nielsen, M. Nielsen, J. M. Tranquada, H. Chou, S. Shamoto, and M. Sato, Phys. Rev. B **41**, 6547 (1990).

[18]J. M. Tranquada, W. J. L. Buyers, H. Chou, T. E. Mason, M. Sato, S. Shamoto, and G. Shirane, Phys. Rev. Lett. **64**, 800 (1990).

[19]M. Sato, S. Shamoto, J. M. Tranquada, G. Shirane, and B. Keimer, Phys. Rev. Lett. **61**, 1317 (1988).

[20]R. F. Kiefl *et al.*, Phys. Rev. Lett. **63**, 2136 (1989).

[21]J. Rossat-Mignod, P. Burlet, M. J. Jurgens, C. Vettier, L. P. Regnault, J. Y. Henry, C. Ayache, L. Forro, H. Noel, M. Potel, P. Gougeon, and J. C. Levet, J. Phys. Colloq. **49**, C8-2119 (1988).

[22]M. J. Jurgens, P. Burlet, C. Vettier, L. P. Regnault, J. Y. Henry, J. Rossat-Mignod, H. Noel, M. Potel, P. Gougeon, and J. C. Levet, Physica B **156-157**, 846 (1989).

[23]S. Tyc, B. I. Halperin, and S. Chakravarty, Phys. Rev. Lett. **62**, 835 (1989).

[24]A. Aharony, R. J. Birgeneau, A. Coniglio, M. A. Kastner, and H. E. Stanley, Phys. Rev. Lett. **60**, 1330 (1988).

[25]H. J. Schulz, Phys. Rev. Lett. **64**, 1445 (1990).

[26]J. M. Tranquada, S. M. Heald, A. R. Moodenbaugh, and Youwen Xu, Phys. Rev. B **38**, 8893 (1988).

[27]Takashi Imai, Tadashi Shimizu, Hiroshi Yasuoka, Yutaka Ueda, and Koji Kosuge, J. Phys. Soc. Jpn. **57**, 2280 (1988).

[28]H. Yasuoka, T. Imai, and T. Shimizu, in *Strong Correlation and Superconductivity,* edited by H. Fukuyama, S. Maekawa, and A. P. Malozemoff (Springer-Verlag, Berlin, 1989).

[29]H. Alloul, T. Ohno, and P. Mendels, Phys. Rev. Lett. **63**, 1700 (1989).

[30]M. Takigawa, A. P. Reyes, P. C. Hammel, J. D. Thompson, R. H. Heffner, Z. Fisk, and K. C. Ott, Phys. Rev. B **43**, 247 (1991).

[31]H. Monien, D. Pines, and M. Takigawa, Phys. Rev. B **43**, 258 (1991).
[32]A. J. Millis, H. Monien, and D. Pines, Phys. Rev. B **42**, 167 (1990).
[33]J. Rossat-Mignod, L. P. Regnault, J. M. Jurgens, P. Burlet, J. Y. Henry, and G. Lapertot, in *Dynamics of Magnetic Fluctuations in High T_c Materials,* edited by G. Reiter, P. Horsch, and G. Psaltakis (Plenum, New York, to be published).
[34]S. R. Renn (private communication).
[35]D. J. Scalapino (private communication).